Journal of Thermal Analysis and Calorimetry
https://doi.org/10.1007/s10973-024-13457-1

A thermal study on NiAl-citrate LDH as catalyst precursor for dry reforming reaction

Marco Fortunato[1] · Marco Piccinni[1] · Andrea Pastorino[1,2] · Anna Maria Cardinale[1]

Received: 15 November 2023 / Accepted: 8 July 2024

Abstract
Ni-based layered double hydroxides (LDHs) are well-known as catalysts precursors; in fact, their properties allow for a homogeneous distribution of Ni on a matrix through simple and economic synthetic passages. In this work, NiAl-citrate LDH was synthetized through a recently developed synthetic pathway that led to the formation of almost single-layered hexagonal nanocrystals. These ones seem to be promising for the production of a Ni (0)-based material with a very high surface area, since through pyrolysis, the interlayered citrate could be turned into CO that simultaneously reduces the Ni (II) to Ni (0) and blow-up the original crystals. In this transformation, temperature plays a key role; therefore, the processes occurring during heating were investigated to discriminate which of them contribute to the material reduction. Additionally, the appropriate pyrolysis temperature was determined to achieve the desired compound that was a homogeneous distribution of nanopatterned micro-flakes of Ni (0) and Al/Ni mixed oxides, with a high specific surface area ($177 m^2 g^{-1}$). The high surface area and the expected properties of this new material make it an interesting candidate for heterogeneous catalysis of high-temperature gas reactions, such as dry reforming, a noteworthy process that produces syngas from the two greenhouse gases CO_2 and CH_4. DRM applicability is limited by high temperatures required to obtain acceptable conversion and by solid carbon deposition on catalyst, both leading to its deactivation over time; so, it is important to develop new catalysts able to overcome those problems. For these purposes, some preliminary tests on the obtained material were performed confirming its catalytic behavior for the DRM, especially at temperatures > 800 K.

Keywords DRM · TG–DTA · LDH · Syngas · Heterogeneous catalysis

Introduction

LDHs are an interesting class of bidimensional layered materials, characterized by a wide range of possible composition and a flexible structure, and their formula is reported in Eq. (1):

$$\left[M^{2+}_{1-x}N^{3+}_{x}(OH)_2\right]^{x+}\left(A^{\frac{n-}{x}}\right)^{x-}\cdot mH_2O \quad (1)$$

M^{2+} is a divalent metal cation, N^{3+} is a trivalent metal cation, A^{n-} is an n-charged anion, X is the molar ratio N/(N + M) and m is a number from 1 to 4 [1].

✉ Marco Fortunato
marco.fortunato@edu.unige.it

[1] Dipartimento di Chimica e Chimica Industriale, Università di Genova, Via Dodecaneso 31, 16146 Genoa, Italy

[2] INSTM UdR di Genova, Via Dodecaneso 31, 16146 Genoa, Italy

The structure of LDHs could be described as a staking of brucite-like layers where part of the Mg^{2+} ions are replaced with a trivalent cation, leading to a positive charge on the surface that is balanced by an interlayered anion.

The structure is a staking of different sheets of $M^{2+}/M^{3+}(OH)_6$ octahedra edge-sharing connected alternately to a layer of anions and water molecules. The structure is stabilized by hydrogen bonds between surface OH groups and interlayered water molecules or anions [1, 2]. A schematic representation of the LDH structure is shown in Fig. 1.

Furthermore, LDHs can be produced with a very wide range of possible synthetic routes to obtain several different micro-structures, from the amorphous bulk obtained by coprecipitation to the very crystalline "flower-like" compound obtained by hydrothermal method [3–5].

Thanks to their interesting properties, LDHs found applications in a bunch of different fields such as catalysis, pollutant recovery, energy storage and everywhere a high exchange capability (of both cations and anions) is required [6–10].

Published online: 08 August 2024

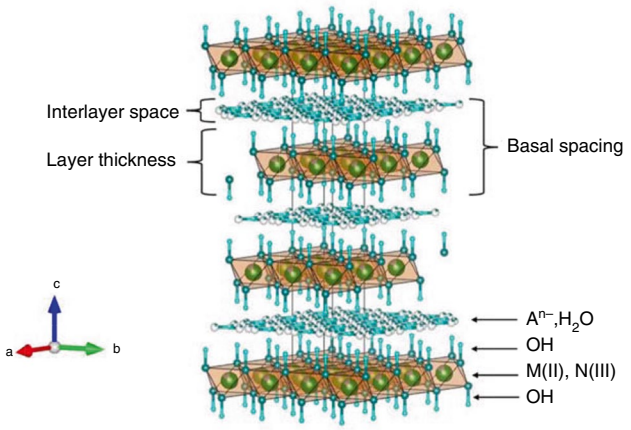

Fig. 1 Schematic representation of the LDH general structure

Until now, in the field of metallic catalysts, all the LDHs containing nickel were used as precursors to obtain a homogeneous distribution of the Ni atoms on a matrix [11, 12]; in particular, NiAl-LDHs seem to be very useful, due to their strong interaction with Al_2O_3 [13, 14]. The properties of these LDH-derived materials make them suitable for catalytic applications, e.g., the Dry Reforming of Methane reaction (DRM).

DRM is an interesting process, as it allows the conversion of two greenhouse gases, CO_2 and CH_4, in syngas, a mixture of H_2 and CO that finds several uses in energy production, in the synthesis of important chemical products and liquid fuels [15, 16]. However, its application at industrial-scale is limited by two main factors: high temperature needed to overcome the reaction endothermicity and reach high conversions (~ 1070 K) and the high cost of the best-performing noble metals catalysts (Ir, Pt and Rh). The use of innovative nickel catalysts for this reaction, active at low temperature and whose prices are far lower than those of noble metals, is thus actively being researched.

The main drawback of nickel for this reaction is represented by the deposition of solid carbon on the catalyst surface as an amorphous layer, nanotubes or whiskers, leading to a temporary or even permanent loss of activity [17].

Until now, in this field, the interlayer anion has played only a structural role; in this work, it was decided to exploit the anion properties to obtain a catalyst with a more microstructured shape and higher surface area instead. NiAl-LDH was synthetized via the hydrolytic polymerization of metal-citrate coordination compounds. This synthesis technique is a modified solvothermal method but produces turbostratic citrate-intercalated LDHs from the restacking of single-layer LDH nanosheets [18, 19]. By heating citrate-intercalated LDHs under anoxic condition, citrate anions decompose into CO that reduces the LDH material into a homogeneous mixture of metallic Ni and Ni/Al mixed oxides. Here, the temperature of pyrolysis plays a key role to obtain the proper micro-structure; in fact, citrate anions must be completely consumed, while the sintering of Ni flakes must be avoided, since that implies a reduction in the catalyst' surface area. Hence, it is pivotal to have a deep understanding of the material behavior under heating, discriminating the different processes occurring at the different mass loss step.

Material and methods

Materials

Aluminum nitrate nonahydrate ($Al(NO_3)_3 \cdot 9H_2O$), nickel acetate tetrahydrate ($Ni(CH_3CO_2)_2 \cdot 4H_2O$), trisodium citrate dihydrate ($Na_3C_6H_5O_7 \cdot 2H_2O$) and sodium hydroxide (NaOH) used for the LDH synthesis were purchased by VWR, Part of Avantor (Leuven, Belgium), with a 98.9% purity. The used water was deionized with an ion exchange unit (M3/M6 Chemical Bürger s.a.s, Genova, Italy), boiled and gurgled with Ar to completely avoid the presence of carbonates and CO_2 in the system.

Methods

Material synthesis

0.4 mmol of $Al(NO_3)_3 \cdot 9H_2O$ (150.0 mg) and 1.2 mmol of $Ni(CH_3CO_2)_2 \cdot 4H_2O$ (298.6 mg) are dissolved into 160 mL of deionized water into a 250mL flask. 1.6 mmol of $Na_3C_6H_5O_7 \cdot 2H_2O$ (470.6 mg) is dissolved into 4 mL of water and then added to the previous solution. The flask is heated to 353 °C for one hour. After heating, the system has cooled down to room temperature, and then 30 mL of 0.1M NaOH solution is added dropwise under vigorous stirring. The whole flask content is transferred into a 250mL round flask and heated to 363 K under reflux and argon atmosphere for 72 h, and then the obtained LDH is collected by centrifugation, at 7000 rpm for 10 min, washed twice with distilled water and dried under vacuum overnight at 313 K.

A portion of the material obtained through this procedure was then annealed at 803 K in a tubular furnace (Carbolite GHA 12/300) for 2 h. The chamber was kept under argon flux for 30 min before starting the heating to eliminate oxygen, and this condition was maintained throughout the experiment.

Characterization

The characterization techniques used were, before and after annealing, X-ray powder diffraction (PXRD), X-ray fluorescence (XRF), field emission scanning electron microscopy

(FE-SEM) and transmission electron microscopy (TEM). The NiAl-citrate LDH was also characterized through a differential thermal analysis–thermogravimetry (DTA–TG), and the specific surface and porosity of the annealed material were investigated through N_2 physisorption at 77 K.

PXRD patterns were recorded using a powder diffractometer (X'Pert MPD, Philips, Almelo, Netherland) equipped with a Cu anticathode ($K_{\alpha 1}Cu = 1.5406$ Å). The indexing of the diffraction data was performed in comparison with the literature for NiAl-citrate. All the other samples were elaborated by full-profile Rietveld refinements, using the software package WinPLOTR [20].

X-ray fluorescence (XRF) analyses were done using a M4 TORNADO micro-XRF Bruker.

DTA/TG analyses were realized with a Labsys Evo 1600–Setaram thermobalance. About 20 mg of sample was placed in an open alumina crucible and heated from 303 to 1523 K, at 10 K min^{-1}, under both Ar and dry air atmosphere (60 mL min^{-1}).

For the transmission electron microscopy was used a JEM 1011–100 kV TEM (W filament thermionic source) by JEOL, and the sample was prepared via the drop-casting of a 1:100 diluted LDH dispersions (approx. 0.001 g L^{-1}) in ethanol onto ultrathin C-on-holey C-coated Cu grids by Ted Pella.

The FE-SEM analysis was done with a ZEISS SUPRA 40 V microscope, and the samples were analyzed by applying an acceleration voltage of 5 kV for 50 s. To further investigate the morphology and porous structure of the material obtained, N_2 physisorption at 77 K was performed with a *Micrometrics ASAP 2020 MP.* The application of BET model allowed to calculate the total surface area of the material.

For the catalytic test, 0.0145 g of catalyst diluted with 0.2519 g of silica sand was used to produce a fixed bed reactor (FBR) in a quartz tube (internal diameter 6 mm; length 0.5 cm) that was put in a laboratory-scale pilot plant where the flow of reactants mixture made of N_2, CO_2 and CH_4 could be controlled through three mass flows (*Bronkhorst EL-FLOW Select*), and the products stream could be measured with a bubble flowmeter and an Agilent 7820A gas-chromatograph with TCD detector. Before the activity test, the catalyst was reduced in situ in a stream of 15 mL min^{-1} of pure hydrogen at 673 K for 30 min. The catalytic evaluation was conducted with 125 mL min^{-1} of a reactant mixture with a 2:2:1 ratio of N_2:CO_2:CH_4 in a temperature range between 673 and 873 K. The CH_4/CO_2 feed ratio of 0.5, lower than stoichiometric value (1), was chosen as it should make the system less prone to carbon deposition phenomena [21].

The percentage concentration of the product i, Ci%, was evaluated through the response factor of TCD (Eq. 2).

$$\mathrm{Ci\%} = \frac{\mathrm{Area_i}}{F_{\mathrm{ri}}} \tag{2}$$

where $\mathrm{Area_i}$ is the chromatographic area of the product i, and F_{ri} is the instrument response factor for each gas.

The molar chromatographic flow, CMP, is calculated from Eq. (3).

$$\mathrm{CMPi}\left[\mathrm{mol\ min^{-1}}\right] = \frac{\frac{Q_{\mathrm{vol\ in}} \cdot \left(\frac{\mathrm{Ci\ \%}}{100}\right)}{1000}}{RT} \tag{3}$$

where $Q_{\mathrm{vol\ in}}$ is the volumetric flow entering reactor $\left[\mathrm{mL\ min^{-1}}\right]$, C% is the percentual concentration, R is the universal gas constant [L mol^{-1} K^{-1}] and T is the absolute temperature [K].

Previous values allow to calculate CH_4 and CO_2 percentage conversion (Eqs. 4 and 5), H_2 percentage yield (Eq. 6) and H_2/CO ratio (Eq. 7).

$$\mathrm{CH_4\%conversion} = \frac{\left(\mathrm{CMP_{CH_4 in}} - \mathrm{CMP_{CH_4 out}}\right) \cdot 100}{\mathrm{CMP_{CH_4 in}}} \tag{4}$$

$$\mathrm{CO_2\%conversion} = \frac{\left(\mathrm{CMP_{CO_2 in}} - \mathrm{CMP_{CO_2 out}}\right) \cdot 100}{\mathrm{CMP_{CO_2 in}}} \tag{5}$$

$$\mathrm{H_2\%Yield} = \frac{\mathrm{CMP_{H_2 out}}}{\mathrm{CMP_{H_2 theoric\ out}}} \cdot 100 = \frac{\mathrm{CMP_{H_2 out}}}{2\mathrm{CMP_{CH_4 in}}} \cdot 100 \tag{6}$$

$$\frac{\mathrm{H_2}}{\mathrm{CO}} = \frac{\mathrm{CMP_{H_2}}}{\mathrm{CMP_{CO}}} \tag{7}$$

Thermodynamic equilibrium values of parameters listed above (Eqs. 4–7), representing theoretical limit that could be reached with an infinite residence time of reactants at a definite temperature inside reactor, were calculated using a software that performs Gibbs free energy minimization. For the present study, it was considered a simplified reaction environment made up only of the main species in gas phase: CO_2, CO, CH_4, H_2, H_2O and N_2.

Results and discussion

NiAl-citrate

Figure 2a shows the typical diffraction pattern of turbostratic LDH materials, with "basal reflections" (00 l) at $2\theta < 30°$, the "fin-like reflections" (0kl) and (h0l) between 30 and 55° and the (110) after 60° [22–24]. The calculated lattice parameters are a = 0.3019 nm and c = 3.669 nm.

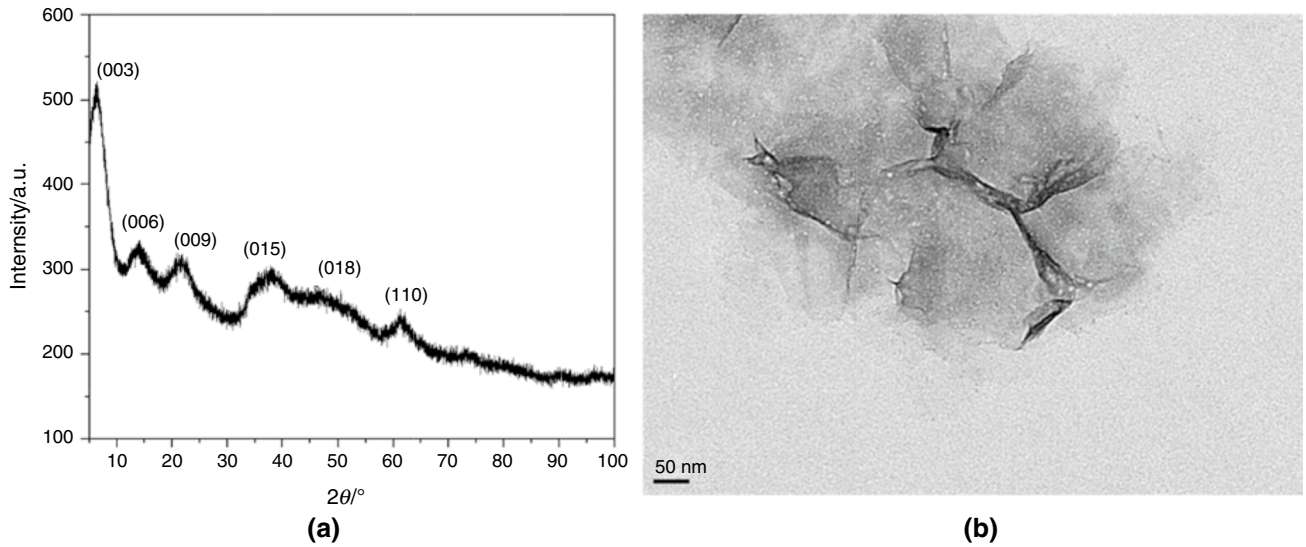

Fig. 2 PXRD pattern **a** and TEM image **b** of NiAl-citrate LDH

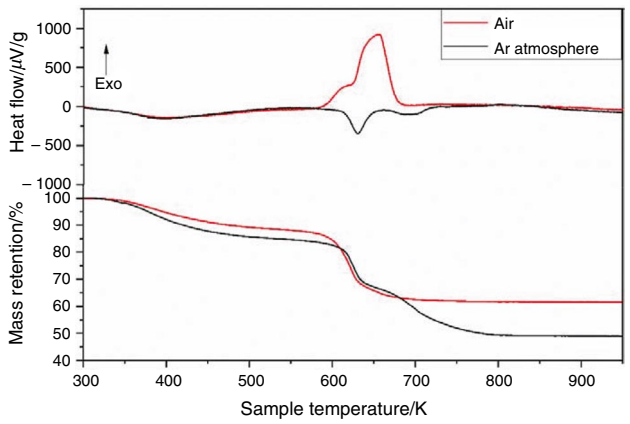

Fig. 3 TG–DTA curve of NiAl-citrate in air (red) and Ar atmosphere (black)

The value of $d_{(003)}$ approximately represents the space occupied by a NiAl octahedron and the interlayer region (basal spacing) [1]. The calculated d values are $d_{(003)}$ NiAl-citrate = 1.223 nm and the interlayer dimension calculated as proposed by Conterosito et al. [25] is 0.743 nm.

The TEM image of the compound (Fig. 2b) reveals an almost single-layer plates constitution, and each plate is approximately 200 nm large and 1–2 nm high as reported by Piccinni et al. [18].

The TG–DTA curve (Fig. 3) in air shows an initial mass loss (13%), from 303 to 593 K, connected with a broad endothermic peak, attributable, as well-known in the literature, to the removal of structural water and not neglectable carbonate impurities [5, 26]; by increasing the temperature, different exothermic processes occur, related to the combustion of the citrate and the conversion of the LDH into oxide (total mass loss: 39%). After the thermal treatment, the material results in a green fine powder, for which PXRD analysis (Fig. 4a) shows the diffraction peaks are well defined and related to the cubic NiO and the spinel-like Al_2NiO_4, in agreement with the literature for other LDHs [26, 27].

Starting from these results and the X-ray fluorescence (XRF) data (SI 1), it is possible to attribute the right amount of crystal water at the LDH formula (Eq. 8).

$$\left[Al_{0.14}Ni_{0.86}(OH)_2\right]\left(NaC_6H_5O_7\right)_{0.07} \cdot H_2O \quad (8)$$

As the TGA under inert atmosphere (Ar) (Fig. 3), the first mass loss (13%) is connected to a broad endothermic peak, and it is, as in the previous sample, due to the dehydration of the LDH.

By carrying on the heating, other two important mass losses occur; the first one between 593 and 703 K leads to a 38% mass loss and is characterized by an endothermic peak, attributable to the conversion of the LDH into oxide and to some rearrangements of the citrate anion. The second, from 703 to 803 K, causes a 55% total mass loss and is connected to an endothermic peak, attributable to the pyrolysis of the citrate with the formation of CO and a subsequent reduction of the metal oxides.

The PXRD analysis of the materials after TGA (Fig. 4b) shows the presence of a main phase recognizable as metallic Ni and e two minority ones attributable to NiO and Al_2NiO_4.

To confirm the hypothesized reactivity under heating, the TG analysis in Ar atmosphere was repeated, in the same condition, stopping the heating at the end of each mass loss

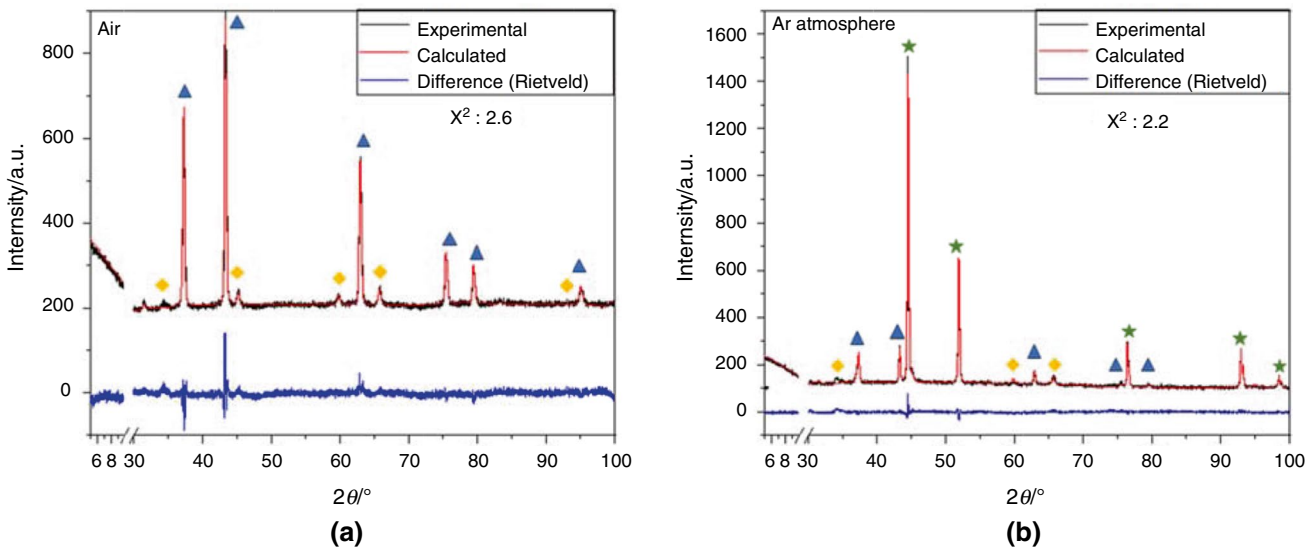

Fig. 4 PXRD pattern of NiAl-citrate after the thermal treatment in dry air **a** and Ar atmosphere **b**, where blue triangles are attributable to NiO, orange rhombus is to $Al_2NiO_4$and green stars are to metallic Ni

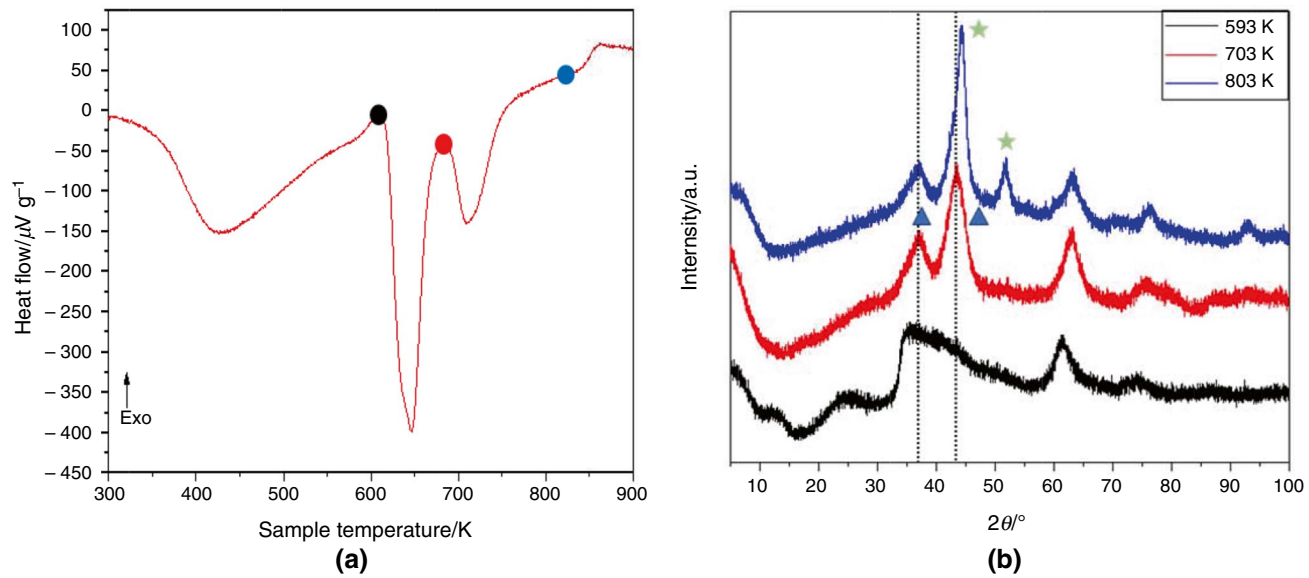

Fig. 5 DTA curve of NiAl-citrate in Ar atmosphere **a** where the colored circles represent the temperature at which the PXRD presented was recorded **b**. Blue triangles represent NiO, and green stars represent metallic Ni

and quickly cooling down the samples (30 K min^{-1}). The so obtained compounds were then characterized by PXRD.

As shown in Fig. 5, the material, immediately after the first endothermal reaction (593 K), shows an amorphous structure, very similar to the pristine LDH, derived from the dehydration and the subsequent distortion of the original structure. After the second step, the material seems to be a mixture of low-crystalline cubic structure oxides (mainly NiO), while at 803 K, the main diffraction peak at 43° disappears and is substituted by two new signals at 44.5 and 55.5° pertaining to metallic Ni. Nickel oxide is still present as demonstrated by the peak at 39° and the left shoulder of the main peak.

NiAl-pyrolyzed

According to the characterization results, a portion of the pristine NiAl-citrate was pyrolyzed at 803 K (immediately after the last endothermic peak); the FE-SEM image (Fig. 6a) shows the nanopatterning of the pyrolyzed

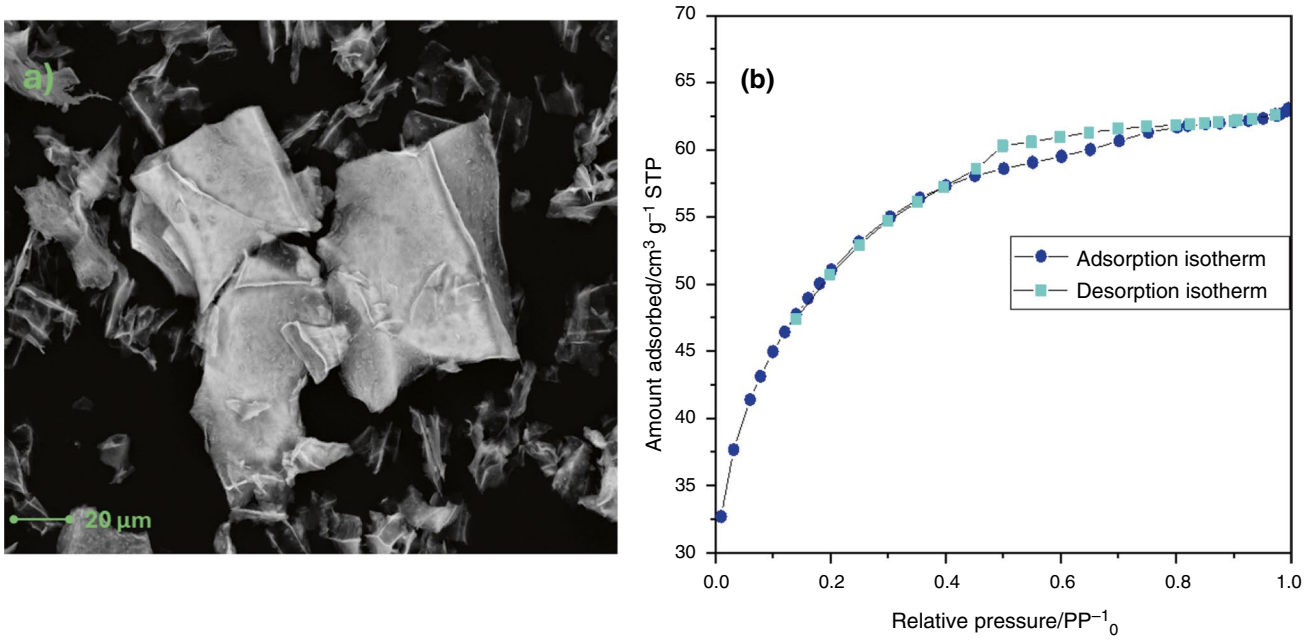

Fig. 6 FE-SEM photograph of NiAl-pyrolyzed **a** and its adsorption (dark blue) and desorption (light blue) isotherms at 77 K **b**

material, and the dimension and shape of the particles are not homogeneous (as expected from an explosive reaction), but it is clear that the material is made up of flakes. Adsorption and desorption isotherms for the material are shown in Fig. 6b, and the shape of isotherms resembles a type I in the IUPAC classification. The presence of a little H4 hysteresis loop indicates that the catalyst has a mesoporosity (2–50 nm) shifted toward low values [28]. The micro-porous shape of the isotherm can be explained by considering the flake structure of the catalyst. The estimated surface area of the material was calculated with a BET model, giving a value of 177 m^2g^{-1}. This value is higher than that obtained by similar catalysts produced from other LDHs where the anions play only a structural role (~ 100–140m^2g^{-1}) and is even comparable with $NiAl_2O_4$ obtained via combustion synthesis (~ 180 m^2g^{-1}) [12, 29, 30].

Some preliminary catalytic tests had been performed, on the pyrolyzed sample, which demonstrated that the material is active for DRM reaction, as proved by the CH_4 mass% conversion, shown in Fig. 7a as a function of reaction temperature. The trend in Fig. 7a reveals that conversion percentage starts almost at zero % up to 823 K and then it starts to increase with temperature up to around 15 mass%. In all the temperature range, the experimental values remain below theoretical thermodynamic equilibrium ones. The yield of the most interesting product, hydrogen,

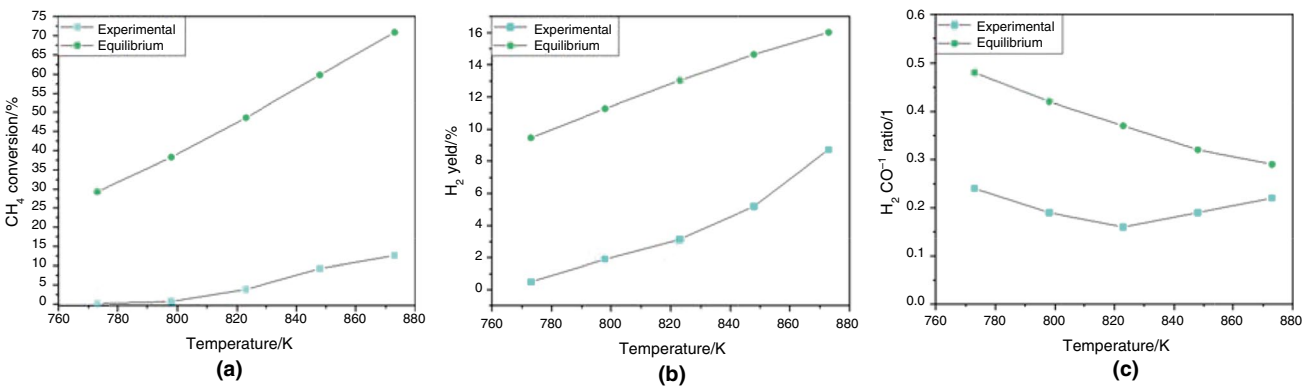

Fig. 7 CH_4% conversion values as a function of reaction temperature **a**. H_2% yield as a function of reaction temperature **b**. H_2/CO ratio in the product stream as a function of reaction temperature **c**. In blue are the displayed experimental values, and in green are the calculated equilibrium ones

has also been calculated, and it is shown in Fig. 7b below. Hydrogen yield seems to increase rapidly with temperature reaching 8% at 880 K. Since the process aim is mainly the production of syngas, the evaluation of the H_2/CO ratio of the gas obtained in this case has been carried out. Figure 7c gives information about the quality of the product and the selectivity of the process, and the values are lower than calculated thermodynamic equilibrium ones. Secondary reactions are taking place and contributing to the decrease in H_2/CO ratio, but the catalyst tends to increase its selectivity toward hydrogen at higher temperatures. The occurrence of the reverse water gas shift reaction probably affects the H_2/CO ratio at the lower temperatures, and probably the catalyst is poorly active toward the methane decomposition which is an endothermic reaction that contributes more to carbon deposition.

Conclusions

In this work, the applicability of the "hydrolytic polymerization" was confirmed also for a different LDH than the e FeNi-citrate reported in the literature [18]. Furthermore, the thermal behavior of NiAl-citrate LDH was deeply investigated discriminating the transformation occurring at each mass loss step, confirming the hypothesis of the role of the citrate as CO generator and its subsequent behavior as reductant for Ni (II) and determining the correct pyrolysis temperature to consume all the citrate and maximize the surface area of the resulting material.

The physisorption measurements showed that the pyrolyzed NiAl-citrate has a quite large BET specific surface area of about 177 m^2g^{-1} and a very specific isotherm of type I, which is related to the flake structure proved by electron microscopy. This area is higher than the one obtained with similar synthetic paths, like the wet impregnation, and is reasonably comparable to the one achievable through much complicated and expensive route like the combustion method.

Finally, it was also demonstrated that the obtained material is active for the DRM reaction, in the preliminary tests, and exhibits a H_2 yield which increased by increasing the temperature. The H_2/CO ratio values are lower than maximum equilibrium ones, but the difference becomes lower at higher temperatures (880 K). Therefore, while the catalyst is still promoting side reactions, it tends to become more selective at higher temperatures.

Supplementary Information The online version contains supplementary material available at https://doi.org/10.1007/s10973-024-13457-1.

Acknowledgements We would like to acknowledge the Laboratory of Electron Microscopy for FE-SEM observations and the membrane&membrane research group for the physisorption measurements at the Department of Chemistry and Industrial Chemistry at University of Genoa.

Author contributions All authors contributed to the study conception and design. The synthesis and characterization of the materials were done by Fortunato M. The surface analysis and catalytic tests were done by Pastorino A. The first draft of the manuscript was written by Fortunato M. And all authors commented on previous versions of the manuscript. All authors read and approved the final manuscript.

Funding Open access funding provided by Università degli Studi di Genova within the CRUI-CARE Agreement.

Declarations

Conflict of interests This paper's authors declare no competing interests.

References

1. Cavani F, Trifirò F, Vaccari A. Hydrotalcite-type anionic clays: preparation, properties and applications. Catal Today. 1991;11(2):173–301. https://doi.org/10.1016/0920-5861(91)80068-K.
2. Li F, Duan X. Applications of Layered Double Hydroxides. In: Duan X, Evans DG, editors. Layered Double Hydroxides. Berlin, Heidelberg: Springer Berlin Heidelberg; 2006. p. 193–223. https://doi.org/10.1007/430_007.
3. He J, Wei M, Li B, Kang Y, Evans DG, Duan X. Preparation of layered double hydroxides. Struct Bond. 2005;119:89–119. https://doi.org/10.1007/430_006.
4. Boclair JW, Braterman PS. Layered double hydroxide stability. 1. Relative stabilities of layered double hydroxides and their simple counterparts. Chem Mater. 1999;11(2):298–302. https://doi.org/10.1021/CM980523U.
5. Conterosito E, et al. Structural characterisation of complex layered double hydroxides and TGA-GC-MS study on thermal response and carbonate contamination in nitrate- and organic-exchanged hydrotalcites. Chem A Eur J. 2015;21(42):14975–86. https://doi.org/10.1002/chem.201500450.
6. Chaillot D, Bennici S, Brendlé J. Layered double hydroxides and LDH-derived materials in chosen environmental applications: a review. Environ Sci Pollut Res. 2020. https://doi.org/10.1007/s11356-020-08498-6.
7. Sikander U, Sufian S, Salam MA. A review of hydrotalcite based catalysts for hydrogen production systems. Int J Hydrog Energy. 2017;42(31):19851–68. https://doi.org/10.1016/J.IJHYDENE.2017.06.089.

8. Mir ZM, Bastos A, Höche D, Zheludkevich ML. Recent advances on the application of layered double hydroxides in concrete—a review. Materials. 2020;13(6):1426. https://doi.org/10.3390/ma13061426.
9. Daud M, et al. A review on the recent advances, challenges and future aspect of layered double hydroxides (LDH)—containing hybrids as promising adsorbents for dyes removal. J Mol Liq. 2019;288: 110989. https://doi.org/10.1016/j.molliq.2019.110989.
10. Tingting H, et al. Layered double hydroxide-based nanomaterials for biomedical applications. Chem Soc Rev. 2022;51(14):6126–76. https://doi.org/10.1039/D2CS00236A.
11. Rosset M, Féris LA, Perez-Lopez OW. Biogas dry reforming using Ni–Al-LDH catalysts reconstructed with Mg and Zn. Int J Hydrog Energy. 2021;46(39):20359–76. https://doi.org/10.1016/J.IJHYDENE.2021.03.150.
12. Tsyganok AI, Tsunoda T, Hamakawa S, Suzuki K, Takehira K, Hayakawa T. Dry reforming of methane over catalysts derived from nickel-containing Mg–Al layered double hydroxides. J Catal. 2003;213(2):191–203. https://doi.org/10.1016/S0021-9517(02)00047-7.
13. Zhan Y, et al. Influence of reduction temperature on Ni particle size and catalytic performance of Ni/Mg(Al)O catalyst for CO2 reforming of CH4. Int J Hydrogen Energy. 2020;45(4):2794–807. https://doi.org/10.1016/J.IJHYDENE.2019.11.181.
14. Xu Y, et al. Improved performance of Ni/Al_2O_3 catalyst deriving from the hydrotalcite precursor synthesized on Al_2O_3 support for dry reforming of methane. Int J Hydrog Energy. 2021;46(27):14301–10. https://doi.org/10.1016/J.IJHYDENE.2021.01.189.
15. le Saché E, Reina TR. Analysis of Dry Reforming as direct route for gas phase CO_2 conversion. The past, the present and future of catalytic DRM technologies. Prog Energy Combust Sci. 2022;89:100970. https://doi.org/10.1016/J.PECS.2021.100970.
16. Hussien AGS, Polychronopoulou K. A review on the different aspects and challenges of the dry reforming of methane (DRM) reaction. Nanomaterials. 2022;12(19):3400. https://doi.org/10.3390/nano12193400.
17. Ranjekar AM, Yadav GD. Dry reforming of methane for syngas production: a review and assessment of catalyst development and efficacy. J Indian Chem Soc. 2021;98(1): 100002. https://doi.org/10.1016/J.JICS.2021.100002.
18. Piccinni M, Bellani S, Bianca G, Bonaccorso F. Nickel–iron layered double hydroxide dispersions in ethanol stabilized by acetate anions. Inorg Chem. 2022;61(11):4598–608. https://doi.org/10.1021/acs.inorgchem.1c03485.
19. Piccinni M Università degli Studi di Genova Istituto Italiano di Tecnologia Doctorate School in Sciences and Technologies of Chemistry and Materials Synthesis, dispersion, electrochemical and optical properties of layered hydroxides nanosheets
20. Roisnel T, Rodríquez-Carvajal J. WinPLOTR: a windows tool for powder diffraction pattern analysis. Mater Sci Forum. 2001;378–381:118–23. https://doi.org/10.4028/www.scientific.net/MSF.378-381.118.
21. Bradford MCJ, Vannice MA. CO_2 reforming of CH_4. Catal Rev. 1999;41(1):1–42. https://doi.org/10.1081/CR-100101948.
22. Forano C, Costantino U, Prévot V, Gueho CT. Chapter 141—Layered double hydroxides (LDH). In: Bergaya F, Lagaly G, editors. Developments in Clay Science. Elsevier; 2013. p. 745–82. https://doi.org/10.1016/B978-0-08-098258-8.00025-0.
23. Sławiński WA, Sjåstad AO, Fjellvåg H. Stacking faults and polytypes for layered double hydroxides: what can we learn from simulated and experimental x-ray powder diffraction data? Inorg Chem. 2016;55(24):12881–9. https://doi.org/10.1021/acs.inorgchem.6b02247.
24. Putman KJ, Rowles MR, Marks NA, Suarez-Martinez I. The role of the 2D-to-3D transition in x-ray diffraction analysis of crystallite size. J Phys Condens Matter. 2021;33(29): 294002. https://doi.org/10.1088/1361-648X/ac0083.
25. Conterosito E, et al. Structural characterization and thermal and chemical stability of bioactive molecule-hydrotalcite (LDH) nanocomposites. Phys Chem Chem Phys. 2013;15(32):13418–33. https://doi.org/10.1039/c3cp51235e.
26. Cardinale AM, Fortunato M, Locardi F, Parodi N. Thermal analysis of MgFe-Cl Layered doubled hydroxide (LDH) directly synthetized and produced 'via memory effect. J Therm Anal Calorim. 2022;147:5297–302. https://doi.org/10.1007/s10973-022-11207-9.
27. Zhang LH, Li F, Evans DG, Duan X. Evolution of structure and performance of Cu-based layered double hydroxides. J Mater Sci. 2010;45(14):3741–51. https://doi.org/10.1007/s10853-010-4423-6.
28. Thommes M, et al. Physisorption of gases, with special reference to the evaluation of surface area and pore size distribution (IUPAC Technical Report). Pure Appl Chem. 2015;87(9–10):1051–69. https://doi.org/10.1515/pac-2014-1117.
29. Rosset M, Féris LA, Perez-Lopez OW. Biogas reforming to syngas over cu-modified Ni-Al-LDH catalysts. Int J Energy Res. 2022;46(15):22664–78. https://doi.org/10.1002/er.8570.
30. Ribeiro NFP, Neto RCR, Moya SF, Souza MMVM, Schmal M. Synthesis of NiAl2O4 with high surface area as precursor of Ni nanoparticles for hydrogen production. Int J Hydrog Energy. 2010;35(21):11725–32. https://doi.org/10.1016/J.IJHYDENE.2010.08.024.